Supplementary Information

Unusual crossover from Bardeen-Cooper-Schrieffer to Bose-Einstein-condensate superconductivity in iron chalcogenides

Yuta Mizukami[1,2], Masahiro Haze[3,4], Ohei Tanaka[1], Kohei Matsuura[1,5], Daiki Sano[3], Jakob Böker[6], Ilya Eremin[6], Shigeru Kasahara[3,7], Yuji Matsuda[3], and Takasada Shibauchi[1]

[1]*Department of Advanced Materials Science, University of Tokyo, Chiba 277-8561, Japan*

[2]*Department of Physics, Tohoku University, 6-3, Aramaki Aza-Aoba, Aoba-ku, Sendai 980-8578, Japan*

[3]*Department of Physics, Kyoto University, Sakyo-ku, Kyoto 606-8502, Japan*

[4]*Institute for Solid State Physics, University of Tokyo, Kashiwa, Chiba 277-8581, Japan*

[5]*Department of Applied Physics, University of Tokyo, Hongo, Bunkyo-ku, Tokyo 113-8656, Japan*

[6]*Institut fur Theoretische Physik III, Ruhr-Universitat Bochum, D-44801 Bochum, Germany*

[7]*Research Institute for Interdisciplinary Science, Okayama University, Okayama 700-8530, Japan*

SUPPLEMENTARY NOTE 1: ENERGY DISPERSIVE X-RAY SPECTROSCOPY (EDX) ANALYSIS

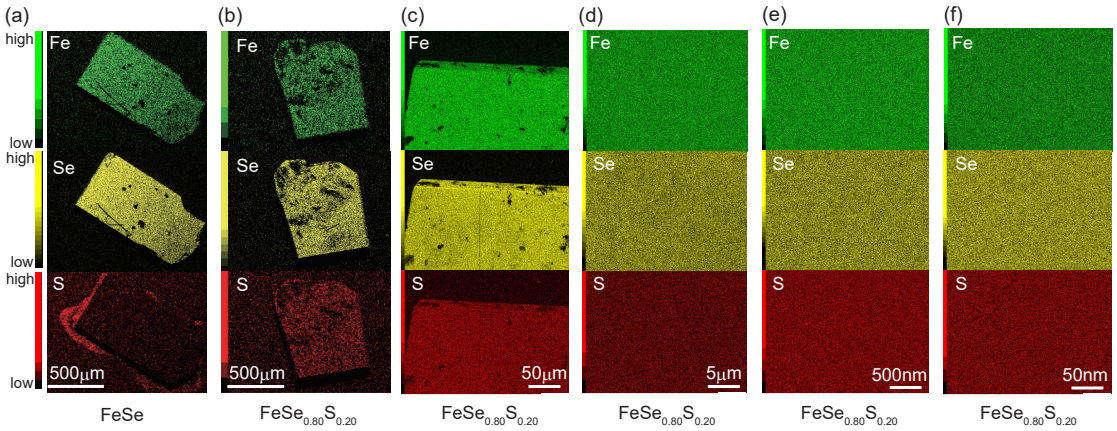

Supplementary Figure 1. Energy Dispersive X-ray spectroscopy (EDX) analysis on tetragonal $FeSe_{0.80}S_{0.20}$ samples in comparison with FeSe. (a) Elemental mapping of Fe (green dots), Se (yellow dots), and S (red dots) at 500 μm scale for $x = 0$. (b)-(f) Elemental mapping of Fe, Se, and S for $x = 0.20$ at the scale of 500 μm((b)), 50 μm((c)), 5 μm((d)), 500 nm((e)), and 50 nm((f)), respectively.

Energy Dispersive X-ray spectroscopy (EDX) analysis is conducted on tetragonal $x = 0.20$ samples in comparison with $x = 0$ to investigate the spatial homogeneity of the sulphur content. For $x = 0$, sulphur intensity is almost same as the background outside the sample position in Supplementary Figure 1(a), showing that there is no sulphur substituted into the sample as expected. Supplementary Figures 1(b)-(f) show the elemental distribution of $x = 0.20$ at the scale of 500 μm, 50 μm, 5 μm, 500 nm, and 50 nm, respectively. Each data shows S intensity with the much thicker color than $x = 0$ although there is some small darker areas in Supplementary Figure 1(b), and (c) which originate from the large impurity attached on the crystal surface and surface roughness in a macroscopic scale and are not from the inhomogeneity of chemical composition. The data at every length scale show the uniform distribution of sulphur which is almost comparable to iron and selenium, indicating that there is no discernible segregation and inhomogeneity down to the mesoscopic scale $\simeq$10 nm. We quantitatively investigate the sulphur content x at the several area inside the sample and the typical variation of x is $\simeq$0.01, demonstrating that such variation of composition cannot explain the results of specific heat and torque measurements.

SUPPLEMENTARY NOTE 2: COMPARISON WITH PREVIOUS HEAT CAPACITY DATA

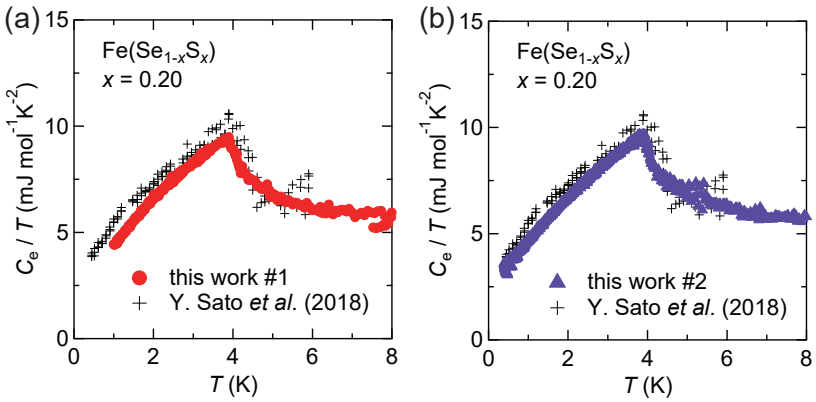

Supplementary Figure 2. Temperature dependence of heat capacity in tetragonal $FeSe_{1-x}S_x$ samples. (a), (b) Temperature dependence of electronic heat capacity divided by temperature for $x = 0.20$ #1 ((a)) and #2 ((b)) in comparison with the data in Refs. [1].

The heat capacity in the tetragonal $FeSe_{1-x}S_x$ has been reported previously by Y. Sato *et al.*, using quasi-adiabatic method[1]. We plot our C_e/T data for two $x = 0.20$ samples in Supplementary Figures 2(a), (b) together with the previous data[1]. The two samples in this work exhibit almost identical temperature dependence and absolute values, indicating the reproducibility of the heat capacity data in $x = 0.20$ with better resolution in our studies. Although the absolute value of our data is slightly smaller than the previous data[1], our data is within the error range of previous data, and both data are basically consistent up to $\simeq 6$ K which is the highest temperature in the previous reports.

SUPPLEMENTARY NOTE 3: UPPER CRITICAL FIELD H_{c2} AND ESTIMATION OF GAUSSIAN FLUCTUATION TERM

The field H dependence of heat capacity is measured in the perpendicular field $H//c$ for $x = 0.0$, and 0.10, and in the perpendicular and parallel field $H//c, ab$ for $x = 0.20$.

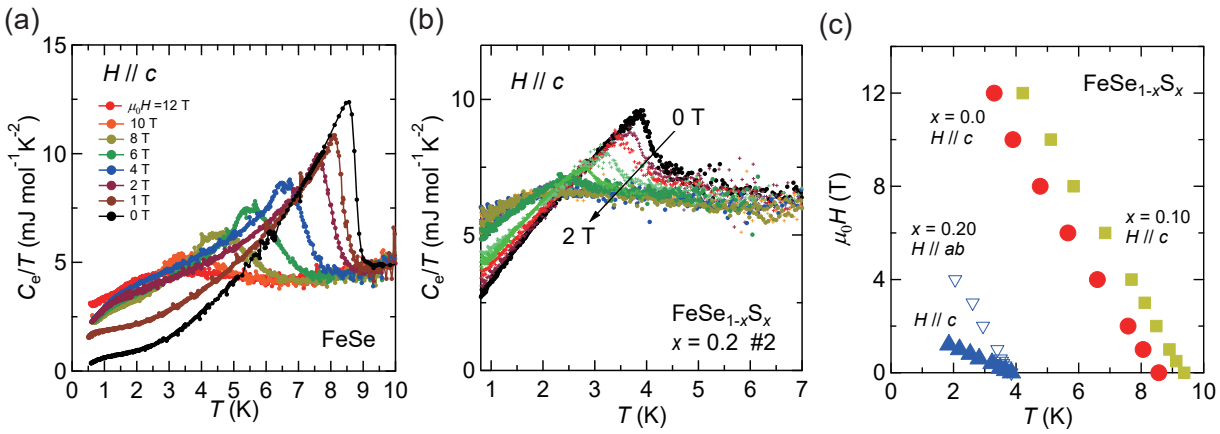

Supplementary Figure 3. Heat capacity in magnetic field for $FeSe_{1-x}S_x$ $x = 0$ and 0.20 and x-dependence of upper critical field. (a), (b) Temperature dependence of electronic heat capacity divided by temperature in magnetic field for $x = 0$ ((a)) and $x = 0.20$ #2 ((b)). The magnetic field is applied along c-axis direction for both samples. (c) Temperature dependence of upper critical field $H_{c2}(T)$ determined from the heat capacity in magnetic field. The $H_{c2}(T)$ for H // ab in $x = 0.20$ and the $H_{c2}(T)$ for H // c in $x = 0.10$ are also plotted in the same panel.

The C_e/T in $H//c$ for several H values are shown for $x = 0.0$ and 0.20 in Supplementary Figures 3(a), (b), respectively. The heat capacity jump due to the superconducting transition becomes broader with increasing H for both S concentrations. This behaviour is possibly due to the enhanced fluctuations in the magnetic field as discussed in $YBa_2Cu_3O_{7-\delta}$[2]. In zero field, we observe the large superconducting fluctuations in heat capacity in $x = 0.20$. The additional heat capacity due to the superconducting fluctuations just above T_c is suppressed by applying magnetic field, and then the C_e/T approaches to the normal state value. This fact indicates that the additional heat capacity responds sensitively to the magnetic field, and does not stem from the incorrect estimation of electronic heat capacity in the normal state when we subtract the lattice contribution. From the T_c defined as the peak temperature in C_e/T under field, we obtain the H-T phase diagram of $x = 0.0$, 0.10 and 0.20 as shown in Supplementary Figure 3(c). In $x = 0.0$ and 0.10 the T-dependence of upper critical field H_{c2} is consistent with previous reports[3, 4], while the H_{c2} for $\mu_0 H > 12$ T cannot be determined from our measurements. The H_{c2} in $x = 0.20$ shows small value compared to $x = 0.0$, reflecting the lower T_c. From the $H_{c2}(0)$ estimated by the WHH

relation $H_{c2}(0) = 0.69T_c|dH_{c2}/dT|_{T=T_c}$[5], we obtain the coherence length $\xi_{ab} = 13.5\,\mathrm{nm}$, $\xi_c = 4.1\,\mathrm{nm}$ for $x = 0.20$ through $H_{c2}(0) = \Phi_0/(2\pi\xi_{ab}^2)$, and $\Phi_0/(2\pi\xi_{ab}\xi_c)$ for $H//c$, and $H//ab$, respectively.

The contribution of the mean field Gaussian fluctuations to the heat capacity [6] is given by $C_{\mathrm{gauss}} = C^+t^{-0.5}$, where $C^+ = k_{\mathrm{B}}/(8\pi\xi_{ab}^2\xi_c)$ and $t \equiv \frac{T-T_{\mathrm{c}}}{T_{\mathrm{c}}}$ is the reduced temperature, and ξ_{ab} and ξ_c are in-plane and out-of-plane coherence lengths at $T = 0$, respectively. The dashed lines in Figs. 4(a) and (b) represent the contribution of Gaussian fluctuations obtained by using $\xi_{ab} = 5.5\,\mathrm{nm}$, $\xi_c = 1.5\,\mathrm{nm}$ for $x = 0$ [7] and $\xi_{ab} = 13.5\,\mathrm{nm}$, $\xi_c = 4.1\,\mathrm{nm}$ for $x = 0.20$.

The Gaussian-type (Aslamasoz-Larkin, AL) fluctuation contribution in susceptibility is given by

$$\chi_{\mathrm{AL}} \approx \frac{2\pi^2}{3}\frac{k_{\mathrm{B}}T_{\mathrm{c}}}{\Phi_0^2}\frac{\xi_{ab}^2}{\xi_c}t^{-\frac{1}{2}} \tag{1}$$

in the zero-field limit. Here Φ_0 is the flux quantum. In the multiband case, the behaviour of χ_{AL} is determined by the shortest coherence length of the main band, which governs the orbital upper critical field. As the diamagnetic contribution χ_{AL} is expected to become smaller in magnitude at higher magnetic fields, $|\chi_{\mathrm{AL}}|$ yields an upper bound for the conventional Gaussian-type amplitude fluctuations.

SUPPLEMENTARY NOTE 4: CALCULATIONS OF PAIRING INSTABILITY AND PAIRING CHANNEL BASED ON THE TWO BAND MODEL

To make an estimate of the splitting between the Cooper-pair formation temperature, T_{pair}, and the actual superconducting transition temperature, T_{c}, we followed previous work[8] and consider a simplified interacting two-band model in two dimensions with hole and electron pockets with small Fermi energies ($E_{\mathrm{F}}^h = 20$ meV and $E_{\mathrm{F}}^e = 10$ meV) as depicted in the Supplementary Figure 4(a). As we are interested in the evolution of the FeSe system as a function of the Sulfur doping we assumed the system is orthorhombic. However, once the intraband interaction in the d-wave interaction dominates and the s-wave component of the gap is small, the results can be easily extrapolated to the purely tetragonal system. The

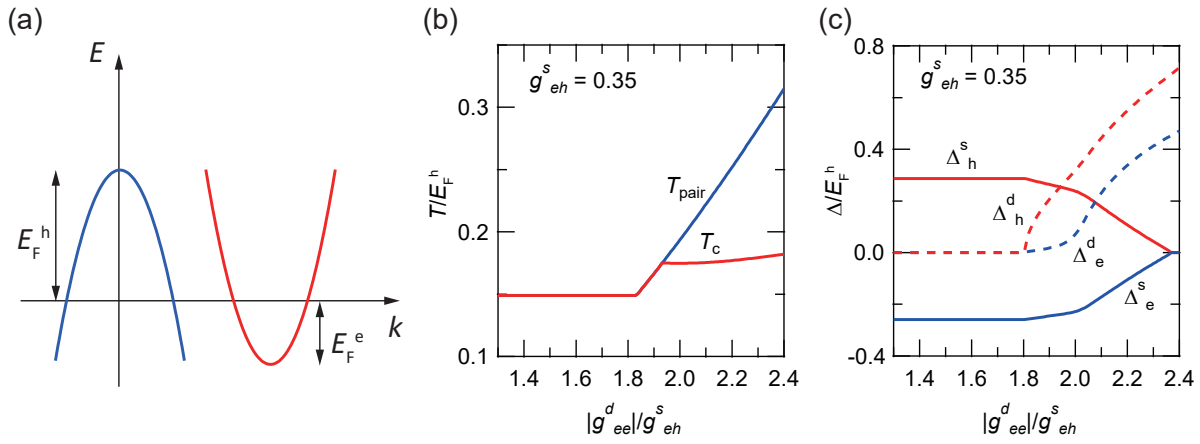

Supplementary Figure 4. Calculation results of pairing and condensation temperature, and intensity of pairing channels based on the two band model. (a) Schematic picture of the assumed electronic structure with hole(blue curve) and electron(red curve) bands. The $E_{\rm F}^h$ and $E_{\rm F}^e$ indicate the Fermi energy of the hole and electron band, respectively. (b) Calculated pairing temperature $T_{\rm pair}$ and condensation temperature $T_{\rm c}$ in units of $E_{\rm F}^h$ as a function of the ratio of intraband to interband interactions in a two-band model. (c) Calculated superconducting gaps in units of $E_{\rm F}^h$ for s-wave and d-wave channels in the electron (e) and hole (h) bands as a function of the ratio of intraband to interband interactions.

Hamiltonian reads

$$\hat{H} = \sum_{\mathbf{k}\alpha\sigma} \xi_{\mathbf{k}\alpha} c^\dagger_{\alpha\mathbf{k}\sigma} c_{\alpha\mathbf{k}\sigma} + \sum_{\mathbf{k},\mathbf{k}',\alpha,\alpha'} U_{\alpha\alpha'}(\mathbf{k}\mathbf{k}') c^\dagger_{\alpha\mathbf{k}\uparrow} c^\dagger_{\alpha-\mathbf{k}\downarrow} c_{\alpha'-\mathbf{k}'\downarrow} c_{\alpha'\mathbf{k}'\uparrow}$$

where $\alpha \in \{e, h\}$, and $\xi_{\mathbf{k}e}$, $\xi_{\mathbf{k}h}$ are the electron and hole energy dispersions separated by the large momentum, respectively as shown in the Supplementary Figure 4(a). Assuming superconductivity due to repulsive interaction in the A_{1g} and B_{2g} symmetry channels, we write the interaction terms as follows

$$U_{\rm eh}(\mathbf{k},\mathbf{k}') = U^s_{\rm eh} + U^d_{\rm eh}\phi(\mathbf{k})\phi(\mathbf{k}')$$
$$U_{\alpha\alpha}(\mathbf{k},\mathbf{k}') = U^d_{\alpha\alpha}\phi(\mathbf{k})\phi(\mathbf{k}')$$

with $\phi(\mathbf{k}) = \cos(2\varphi) = \frac{k_x^2 - k_y^2}{k_x^2 + k_y^2}$. Here, we further assume that the inter-band repulsion drives $s^\pm$-wave symmetry of the superconducting order parameter, while interaction in the d-wave

channel is mostly intra-band. We define superconducting order parameters as

$$\Delta_\alpha(\mathbf{k}) = \sum_{\mathbf{k}',\alpha\prime} U_{\alpha\alpha\prime}(\mathbf{k},\mathbf{k}')\langle c_{\alpha'-\mathbf{k}'\downarrow} c_{\alpha'\mathbf{k}'\uparrow}\rangle \tag{2}$$

and perform a mean-field decoupling to find the mean-field gap equations

$$\begin{aligned}
\Delta^s_{\rm e} =& - g^s_{\rm eh}\int_0^{2\pi}\frac{d\varphi}{2\pi}\int_0^{\Lambda} d\epsilon \frac{\tanh\left(\frac{E_{\rm e}(\mathbf{k})}{2T}\right)}{2E_{\rm e}(\mathbf{k})}\\
\Delta^s_{\rm h} =& - g^s_{\rm eh}\int_0^{2\pi}\frac{d\varphi}{2\pi}\int_0^{\Lambda} d\epsilon \frac{\tanh\left(\frac{E_{\rm h}(\mathbf{k})}{2T}\right)}{2E_{\rm h}(\mathbf{k})}\\
\Delta^d_{\rm e} =& |g^d_{\rm ee}|\int_0^{2\pi}\frac{d\varphi}{2\pi}\int_0^{\Lambda} d\epsilon \frac{\cos^2(\varphi)\tanh\left(\frac{E_{\rm e}(\mathbf{k})}{2T}\right)}{2E_{\rm e}(\mathbf{k})}\\
& - g^d_{\rm eh}\int_0^{2\pi}\frac{d\varphi}{2\pi}\int_0^{\Lambda} d\epsilon \frac{\cos^2(\varphi)\tanh\left(\frac{E_{\rm h}(\mathbf{k})}{2T}\right)}{2E_{\rm h}(\mathbf{k})}\\
\Delta^d_{\rm h} =& |g^d_{\rm hh}|\int_0^{2\pi}\frac{d\varphi}{2\pi}\int_0^{\Lambda} d\epsilon \frac{\cos^2(\varphi)\tanh\left(\frac{E_{\rm h}(\mathbf{k})}{2T}\right)}{2E_{\rm h}(\mathbf{k})}\\
& - g^d_{\rm eh}\int_0^{2\pi}\frac{d\varphi}{2\pi}\int_0^{\Lambda} d\epsilon \frac{\cos^2(\varphi)\tanh\left(\frac{E_{\rm e}(\mathbf{k})}{2T}\right)}{2E_{\rm e}(\mathbf{k})}.
\end{aligned} \tag{3}$$

The dimensionless coupling constants are now given by dimensionless $g_{\alpha\alpha\prime} = N_0 U_{\alpha\alpha\prime}$ with the density of states in two dimensions $N_0 = \frac{m}{2\pi}$. $\Lambda = 1\text{eV} \gg E^h_{\rm F}$ is the high energy cut-off and $E_\alpha(\mathbf{k}) = \sqrt{\xi^2_\alpha + \left[\Delta^s_\alpha + \Delta^d_\alpha \cos(\varphi)\right]^2}$ is the energy dispersion of the Bogoliubov quasiparticles. Note that while the inter-band term between electron and hole pockets is assumed to be repulsive, the intraband $g^d_{\rm ee} < 0$ and $g^d_{\rm hh} < 0$ are attractive in the d-wave channels. In case of $\Delta_\alpha/E^\alpha_{\rm F} \sim 1$, where $E^\alpha_{\rm F}$ ($\alpha \in \{e,h\}$) is the Fermi energy of each band, we need to renormalize the chemical potential assuming the total number of particles is conserved. The equation determining the particle number is given by

$$\begin{aligned}
E^e_{\rm F} - E^h_{\rm F} =& -\int_0^{2\pi}\frac{d\varphi}{2\pi}\int_0^{\Lambda} d\epsilon\\
& \left(\frac{\xi_e(\mathbf{k})\tanh\left(\frac{E_{\rm e}(\mathbf{k})}{2T}\right)}{2E_{\rm e}(\mathbf{k})} + \frac{\xi_h(\mathbf{k})\tanh\left(\frac{E_{\rm h}(\mathbf{k})}{2T}\right)}{2E_{\rm h}(\mathbf{k})}\right)
\end{aligned} \tag{4}$$

and it has to be solved self-consistently with Eqs.(3). The pair building temperature $T_{\rm pair}$ at which electrons form Cooper pairs can be obtained from the condition that the determinant

in

$$0 = -\begin{pmatrix} 1 & g^s_{\rm eh}\Pi^s_h & & & \\ g^s_{\rm eh}\Pi^s_e & 1 & & & \\ & & 1-|g^d_{\rm ee}|\Pi^s_e & g^d_{\rm eh}\Pi^d_e & \\ & & g^d_{\rm eh}\Pi^d_e & 1-|g^d_{\rm hh}|\Pi^s_h & \end{pmatrix}\begin{pmatrix} \Delta^s_{\rm e} \\ \Delta^s_{\rm h} \\ \Delta^d_{\rm e} \\ \Delta^d_{\rm h} \end{pmatrix} \tag{5}$$

vanishes and

$$\Pi^s_\alpha = \int_0^{2\pi}\frac{d\varphi}{2\pi}\int_0^\Lambda d\epsilon \frac{\tanh\left(\frac{\xi_\alpha}{2T_{\rm pair}}\right)}{2\xi_\alpha} \tag{6}$$

$$\Pi^d_\alpha = \int_0^{2\pi}\frac{d\varphi}{2\pi}\int_0^\Lambda d\epsilon \frac{\cos^2(2\varphi)\tanh\left(\frac{\xi_\alpha}{2T_{\rm pair}}\right)}{2\xi_\alpha}. \tag{7}$$

In the usual BCS case the phase fluctuations are costly and $T_{\rm c} \approx T_{\rm pair}$. In our case due to smallness of the Fermi energies, the condensation of pairs may happen at lower temperature, $T_{\rm c} \leq T_{\rm pair}$. We estimate $T_{\rm c} \approx \frac{\pi}{2}\rho_{\rm s}$ where $\rho_{\rm s}(T=0)$ is the superfluid-stiffness following the previous work[8]. Note that in two dimensions, the superconducting transition temperature is $T_{\rm c} \sim \rho_s(T_{\rm c})$ (see, e.g., the references[9, 10].). The interplay between $T_{\rm c}$ and $T_{\rm pair}$ depends on the ratio $\rho_s(T=0)/T_{\rm pair}$. If this ratio is large, the superfluid stiffness rapidly increases below $T_{\rm pair}$. In this situation, $T_{\rm c} = T_{\rm pair}$ minus a small correction, i.e., the phases of bound pairs order almost immediately after the pairs develop (phase fluctuations cost too much energy). If $\rho_s(T=0)/T_{\rm pair}$ is small, $\rho_s(T)$ increases slowly below $T_{\rm pair}$ and $T_{\rm c}$ is of order $\rho_s(T=0)$. In the previous work[8], its expression was extended to the multiband case where $\rho_{\rm s}$ is given by $\rho_{\rm s} \approx \rho_{\rm e} + \rho_{\rm h}$,

$$\rho_{\rm e} = \frac{1}{16\pi^2}\int_0^{2\pi} d\varphi \int_0^\Lambda d\epsilon \Delta^2_{\rm e}\frac{\epsilon}{E_{\rm e}(\mathbf{k})^3} \tag{8}$$

$$\rho_{\rm h} = \frac{1}{16\pi^2}\int_0^{2\pi} d\varphi \int_0^\Lambda d\epsilon \Delta^2_{\rm h}\frac{\epsilon}{E_{\rm h}(\mathbf{k})^3}. \tag{9}$$

We solved Eqs. (3) together with Eq. (4) for the mixed $s+d$-wave gaps in the orthorhombic state at $T=0$ and used them as an input parameter to calculate $T_{\rm c}$. The Cooper-pair formation temperature, $T_{\rm pair}$ is found from the condition that the determinant in Eq. (5) vanishes and the results are shown in the Supplementary Figure 4(b) in units of $E^h_{\rm F}$. The pair-formation temperature $T_{\rm pair}$ and condensation temperature $T_{\rm c}$ are calculated as a function of the ratio of intraband and interband interactions $|g^d_{\rm ee}|/g^s_{\rm eh}$ shown in Supplementary Figure 4(b). The two temperatures split and the difference grows with increasing $|g^d_{\rm ee}|/g^s_{\rm eh}$.

Supplementary Figure 4(c) shows the evolution of the gap symmetry as a function of $|g^d_{\rm ee}|/g^s_{\rm eh}$ also in units of $E^h_{\rm F}$, and we can see the dominant d-wave character for each band with large $|g^d_{\rm ee}|/g^s_{\rm eh}$ regime. Note that for smaller ratio of $|g^d_{ee}|/g^s_{eh}$ the pairing symmetry is a pure s^{+-} driven by inter-band interactions. In this case both gaps are equal in magnitude, but with the larger gap at the band with smaller $E_{\rm F}$. With increasing intra-band coupling in the d-wave gaps Δ^d_e and Δ^d_h grow while the s-wave gaps become smaller. Since we assume $|g^d_{ee}| \gg g^d_{eh}$, Δ^d_e and Δ^d_h differ in magnitude with the larger gap at the band with larger $E_{\rm F}$.

Supplementary References

[1] Sato, Y. *et al.* Abrupt change of the superconducting gap structure at the nematic quantum critical point in $FeSe_{1-x}S_x$. *Proc. Natl. Acad. Sci. U.S.A.* **115**, 1227-1231 (2018).

[2] Overend, N., Howson, M. A. and Lawrie, I. D. 3D X-Y Scaling of the Specific Heat of $YBa_2Cu_3O_{7-\delta}$ Single Crystals. *Phys. Rev. Lett.* **72**, 3238-3241 (1994).

[3] Muratov, A. V. *et al.* Specific heat of FeSe: Two gaps with different anisotropy in superconducting state. *Physica B* **536**, 785-789 (2018).

[4] Abdel-Hafiez, M. *et al.* Superconducting properties of sulfur-doped iron selenide. *Phys. Rev. B* **91**, 165109 (2015).

[5] Werthamer, N. R., Helfand, E. and Hohenberg, P. C. Temperature and Purity Dependence of the Superconducting Critical Field, H_{c2} III. Electron Spin and Spin-Orbit Effects. *Phys. Rev.* **147**, 295-302 (1966).

[6] Inderhees, S. E. *et al.* Specific heat of single crystals of $YBa_2Cu_3O_{7-\delta}$: Fluctuation effects in a bulk superconductor. *Phys. Rev. Lett.* **60**, 1178-1180 (1988).

[7] Kasahara, S. *et al.* Giant superconducting fluctuations in the compensated semimetal FeSe at the BCS-BEC crossover. *Nat. Commun.* **7**, 12843 (2016).

[8] Chubukov, A. V., Eremin, I. and Efremov, D. V. Superconductivity versus bound-state formation in a two-band superconductor with small Fermi energy: Applications to Fe pnictides/chalcogenides and doped $SrTiO_3$. *Phys. Rev. B* **93**, 174516 (2016).

[9] Pokrovsky, V. L. Properties of ordered, continuously degenerate system, *Adv. Phys.* **28**, 595 (1979).

[10] Beasley, M. R., Mooij, J. E. and Orlando, T. P. Possibility of Vortex-Antivortex Pair Dissociation in Two-dimensional Superconductors, *Phys. Rev. Lett.* **42**, 1165 (1979).